ELSEVIER

International Journal of Heat and Fluid Flow 23 (2002) 258–268

International Journal of HEAT AND FLUID FLOW

www.elsevier.com/locate/ijhff

A computational study of binary alloy solidification in the MEPHISTO experiment ☆

V. Timchenko [a], P.Y.P. Chen [a], E. Leonardi [a], G. de Vahl Davis [a,*], R. Abbaschian [b]

[a] *School of Mechanical and Manufacturing Engineering, The University of New South Wales, Sydney, NSW 2052, Australia*
[b] *The University of Florida, Gainsville, FL 32611, USA*

Abstract

A computational model is presented for the study of the solidification of a binary alloy. The enthalpy method has been modified and incorporated into both an in-house code SOLCON (Heat Transfer 98, 1998, p. 241) and the commercial CFD code CFX (CFX 4.2: Solver, 1997). The model has been used to simulate experiments on solidification of a bismuth–tin alloy which were performed during the 1997 flight of the MEPHISTO-4 experiment on the US Space Shuttle Columbia. The effects of thermal and solutal convection in the microgravity environment and of concentration-dependent melting temperature on the phase change processes are included. Comparisons of numerical solutions with actual microprobe results obtained from the MEPHISTO experiments are presented. © 2002 Published by Elsevier Science Inc.

Keywords: Solidification; Binary alloy; Microgravity; Bridgman furnace; MEPHISTO experiment

1. Introduction

The study of solidification processes is very important for the growth of high quality crystals. The performance of electronic devices strongly depends on the presence of microscopic crystal defects and compositional variations caused by convection effects. The MEPHISTO [1] experiment was a cooperative US–French–Australian research effort directed towards gaining a detailed understanding of crystal growth with reference to the solidification behaviour of Bi-1 at.% Sn alloy. It combined ground-based experiments and a series of experiments conducted in a microgravity environment so that convection was decreased to a level at which crystal growth was largely diffusion controlled. The latest MEPHISTO experiment was performed on board the US Space Shuttle *Columbia* during the USMP-4 [2] mission in November–December 1997.

The MEPHISTO-4 apparatus, shown schematically in Fig. 1, consists of three parallel tubes or ampoules (only one is shown in the figure), each containing some sample material, around which are placed two "furnaces", each comprising a pair of heating and cooling jackets. Between each heating and cooling jacket is a nominally adiabatic or insulated zone. One furnace is fixed, and acts to generate a reference state; the other can be moved over the tubes. If it moves in the direction from the cooling to the heating jacket (i.e., to the right in Fig. 1), the material will be progressively solidified from left to right; when it moves in the opposite direction, melting will take place.

The in-flight experiment, which lasted for almost 14 days, consisted of a series of "events", most of which contained three phases: solidification, holding and melting. The solid/liquid (s/l) interface advanced progressively along the ampoule over a period of about a week, during which a number of events at different solidification and melting speeds ranging from 0.74 to 40 μm/s, and lasting for periods of up to several hours occurred. During the following week, the procedure was reversed, culminating in a rapid quenching of the alloy

☆ This paper is a revised and expanded version of a paper presented at CHT'01, the Second International Symposium on Advances in Computational Heat Transfer (Palm Cove, Qld., Australia, 20–25 May 2001), the proceedings of which were published by Begell House, Inc.

* Corresponding author. Tel.: +61-2-9385-4099; fax: +61-2-9663-1222.

E-mail address: g.devahldavis@unsw.edu.au (G. de Vahl Davis).

[1] Matériel pour l'Etude des Phenomènes Intérrasants de la Solidification sur Terre et en Orbite.

[2] United States Microgravity Payload.

0142-727X/02/$ - see front matter © 2002 Published by Elsevier Science Inc.
PII: S0142-727X(02)00173-X

Nomenclature

c_p	specific heat at constant pressure
C	solute concentration
D	solute diffusivity
f	volume fraction
g	gravitational acceleration
h	enthalpy
H	ampoule height
k	thermal conductivity
k_p	partition coefficient
p	iteration number
q	heat flux
t	time
T	temperature
T_m	melting temperature
V	velocity
u	velocity component in x direction
v	velocity component in y direction

Greeks

β_C	solutal expansion coefficient
β_T	thermal expansion coefficient
Δx	mesh size in x direction
Δy	mesh size in y direction
ρ	density
ψ	stream function
ζ	vorticity
μ	dynamic viscosity

Subscripts

a	analytical
amp	ampoule
b	boundary
h	hot zone
I	interface
i, j	grid point
l	liquid
n	numerical
r	reference value
s	solid
w	wall
ϕ	phase

Superscripts

$\sim$	vector
k	time step
p	inner iteration

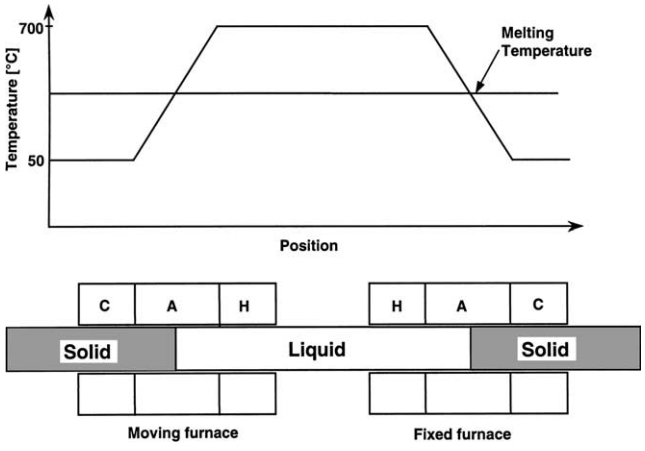

Fig. 1. Schematic diagram of the MEPHISTO apparatus, and the nominal boundary temperature distribution. H and C denote the hot and cold sections of the furnaces; A denotes the adiabatic zone.

to preserve the interface composition and shape for post-flight analysis. Among the objectives of the experiment were:

- determination of the s/l interface temperature using a Seebeck technique (Rouzaud et al., 1988) in which the differential voltage between the stationary and moving interfaces was measured,
- determination of the s/l interface shape using a Peltier pulse technique.

Part of the MEPHISTO program was the numerical modelling of the solidification process. Numerical simulations allow the investigation of the effects of natural convection on the interface shape, the prediction of planar (i.e., non-dendritic) front instabilities and the calculation of the segregation or redistribution of solute during solidification. Numerical simulations have become an important part of the post-flight analysis providing a better interpretation of experimental data and the determination of the property values of bismuth.

For modelling transient phase change processes, a fixed-grid single domain approach is widely accepted to be simpler and lower in computational cost than front tracking methods. However, the standard fixed-grid enthalpy formulation has a major weakness: it produces spurious numerical oscillations in the predicted temperature and interface positions. To overcome this oscillatory behaviour, Voller and Fabbri (1995) suggested selecting only predictions that occur when the interface crosses over a node point. Tacke (1985) employed a special discretization of the heat fluxes which allowed the removal of the numerical oscillations for a *one-dimensional* phase change problem. Laouadi et al. (1998) developed a numerical method based on averaging the microscopic conservation equations of a two-phase composite medium over a control volume with the assumption that the phases may coexist at a temperature different from the melting temperature.

The problem becomes more complex for isothermal plane front (i.e., non-dendritic [3]) solidification of binary alloys. The severe discontinuity of solute concentration at the s/l interface and the sharp gradients of concentration near the interface induced by the low values of both the diffusion coefficient for tin in bismuth and the partition coefficient of tin require special treatment of the diffusion flux at the interface to obtain accurate solutions. Additional difficulties arise when the effect of solute concentration on melting temperature is taken into consideration and the s/l interface position becomes dependant on concentration as well as temperature. Accurate estimation of interface concentration during plane front solidification becomes essential to obtain a smooth history of the interface position.

In this paper we describe a modification of the fixed-grid approach for the study of unidirectional plane front solidification of a Bi-1 at.% Sn alloy in a Bridgman furnace. Thermal conductivity differences between the solid and liquid phases are included. We first describe the mathematical model of the solidification process and then the formulations and procedures required to solve such a model numerically. Finally the model is applied to the simulation of some of the MEPHISTO events. The problem involves heat conduction in the solid alloy and in the walls of the ampoule containing the alloy; thermal and solutal convection; and diffusion in the liquid. Solute diffusion in the solid is neglected. The effects of concentration-dependent melting temperature on the phase change processes are incorporated.

2. Mathematical formulation and numerical model

The governing time dependent equations describing mass, momentum, heat and solute transport in the vorticity–stream function formulation are:

$$\rho\left(\frac{\partial\zeta}{\partial t}+\nabla\cdot(\widetilde{V}\zeta)\right)=\nabla\rho\times\hat{g}|g|+\mu\nabla^2\zeta \tag{1}$$

$$\nabla^2\psi=-\zeta \tag{2}$$

$$\rho c_p\left(\frac{\partial T}{\partial t}+\nabla.(\widetilde{V}T)\right)=k\nabla^2T \tag{3}$$

$$\frac{\partial C}{\partial t}+\nabla\cdot(\widetilde{V}C)=D\nabla^2C \tag{4}$$

where ρ, μ, c_p, k and D are respectively the density, viscosity, specific heat and thermal conductivity of the alloy and the diffusivity of the solute; ζ, ψ, T, $\widetilde{V}$ and C are respectively the vorticity, stream function, temperature, velocity vector and solute concentration; g is the magnitude of the gravitational acceleration, and $\hat{g}$ is the unit vector in the direction of gravity. The density in the buoyancy term of Eq. (1) is assumed to be a linear function of temperature and solute concentration:

$$\rho=\rho_{\mathrm{r}}[1-\beta_T(T-T_{\mathrm{r}})+\beta_C(C-C_{\mathrm{r}})] \tag{5}$$

where β_T and β_C are the (assumed constant) thermal and solutal expansion coefficients, defined by

$$\beta_T=-\frac{1}{\rho_r}\frac{\partial\rho}{\partial T} \tag{6}$$

and

$$\beta_C=\frac{1}{\rho_r}\frac{\partial\rho}{\partial C} \tag{7}$$

ρ_{r}, T_{r} and C_{r} are reference values of density, temperature and concentration.

2.1. Fixed-grid numerical formulation for phase change problems

To account for solidification of a binary alloy, the movement of the s/l interface leading to the evolution of latent heat and release of solute near the interface has to be incorporated in the mathematical model. Using a fixed grid in a single domain that does not change in size and shape, the time-consuming explicit tracking of the movement of the interface is replaced by a less demanding problem in which appropriate source terms in the energy and solute equations take the place of the boundary conditions at the interface. The computational domain comprises either "liquid" or "solid" or "partially solidified" cells; it is only for the latter that the source terms are not zero. As far as flow is concerned, all computational cells are treated as either "liquid" or "solid" cells depending on whether the interface has passed the grid point located at the centre of the control volume. The exact location of the interface is not known a priori and must be determined as part of the solution process from the computed temperature and concentration. We assume a vertical interface in each control volume, the position of which is determined by the calculated local liquid fraction (details of this calculation appear in the next section). Overall the interface is reconstructed by connecting these vertical lines in the mid-height of control volumes and in general can have any shape. In the microgravity environment considered here, the interface is almost vertical, with only a slight curvature near the boundaries.

2.1.1. Energy equation and procedure for liquid fraction calculation

With the assumption that specific heat $c_{p\phi}$ is constant in each phase (ϕ), the enthalpy can be written as the sum of the sensible and latent heat:

$$h=c_{p\phi}T+f_{\mathrm{l}}L \tag{8}$$

[3] The front is not actually planar, but the term is used by materials scientists for morphologically stable, non-cellular solidification.

in which L is the latent heat and f_l is the local liquid fraction. Substitution of Eq. (8) into the energy Eq. (3) yields

$$\rho c_{p\phi}\left(\frac{\partial T}{\partial t}+\nabla\cdot(\widetilde{V}T)\right)=\nabla\cdot(k\nabla T)+S_T \tag{9}$$

where

$$S_T=-\frac{\partial}{\partial t}(\rho f_l L) \tag{10}$$

The source term (10) is used to account for latent heat release during phase change. For a partially solidified cell, a weighted average control volume conductivity is calculated from:

$$k_{i,j}=\frac{k_l k_s}{f_s k_l+f_l k_s} \tag{11}$$

where subscripts 's' and 'l' refer to the solid and liquid phases.

Eqs. (8)–(10) represent the fixed-grid approach for modelling heat transfer during a phase change. An essential part of this approach is the derivation of an enthalpy–temperature–liquid fraction relationship. Standard enthalpy methods are known to produce oscillations in temperature due to the fact that the nodal temperature of a partially solidified control volume is assumed to be constant (equal to the melting temperature) while the liquid fraction, and hence the enthalpy are changing. To overcome this problem (Timchenko et al., 2000) we chose the temperature variation for the nodal temperature of the partially solidified control volume to represent the range over which solidification of this cell occurs (i.e., as the liquid fraction varies from 1 to 0) due to boundary temperature profile translation; this variation was based on the constant temperature slope across a solidifying cell in the direction of solidification. If the cell boundary temperatures in the direction of crystal growth are $T_{i-1/2,j}$ and $T_{i+1/2,j}$ respectively, and the melting point is T_m, the liquid fraction f_l is given by $f_l=(T_{i+1/2,j}-T_m)/(T_{i+1/2,j}-T_{i-1/2,j})$ so that a cell starts to solidify when the interface crosses the left cell boundary ($T_{i-1/2,j}\leqslant T_m$) and becomes completely solid when the interface crosses the right cell boundary ($T_{i+1/2,j}\leqslant T_m$). However, this approach is effective only if the liquid and solid conductivities are equal or nearly the same.

In the case of unequal thermal conductivities in the solid and liquid phases, which is the case here, the temperature gradient across a solidifying cell in the direction of solidification cannot be assumed to be constant, and the expression for liquid fraction derived in Timchenko et al. (2000) is no longer valid. To obtain a smooth history of the temperature and interface position and to account for the change in the temperature gradient while the interface travels over the solidifying cell, a weighting procedure for the estimation of liquid fraction in a partially solidified control volume is proposed. The weighting in this scheme is designed to avoid a discontinuity when the interface passes the grid point and also when it goes from one cell to the next. It provides a smooth transition in the temperature gradient based on which liquid fraction is calculated and hence in the rate of solidification while solidifying.

Based on temperatures at the current iteration, two liquid fractions based on the temperature gradients west and east of the (i, j) cell shown in Fig. 2 can be found:

$$f_l|_w=1.0-\frac{T_m-0.5(T_{i-1,j}+T_{i,j})}{T_{i,j}-T_{i-1,j}} \tag{12}$$

$$f_l|_e=\frac{0.5(T_{i+1,j}+T_{i,j})-T_m}{T_{i+1,j}-T_{i,j}} \tag{13}$$

A weighting based on the value of liquid fraction from the previous iteration is then applied:

$$f_l^p=f_l^{p-1}f_l|_w+(1-f_l^{p-1})f_l|_e \tag{14}$$

where p is the iteration number. As in the case with equal thermal conductivities (and hence a constant temperature gradient in the direction of solidification) the cell starts to solidify when

$$T_{i-1/2,j}=0.5(T_{i-1,j}+T_{i,j})=T_m \quad \text{and} \quad f_l|_w=1$$

and becomes completely solid when

$$T_{i+1/2,j}=0.5(T_{i+1,j}+T_{i,j})=T_m \quad \text{and} \quad f_l|_e=0$$

In between, while $T_{i-1/2,j}<T_m<T_{i+1/2,j}$, the liquid fraction of the partially solidified cell is calculated from the weighted average of the temperature gradients in the liquid and solid. It should be noted that the scheme described by Eqs. (12) and (13) is applicable only for a uniform grid, and requires modification if a non-uniform grid is used.

As it is unlikely that the interface will coincide with the cell boundary at the last time step before the cell is completely solidified, it is proposed that the liquid

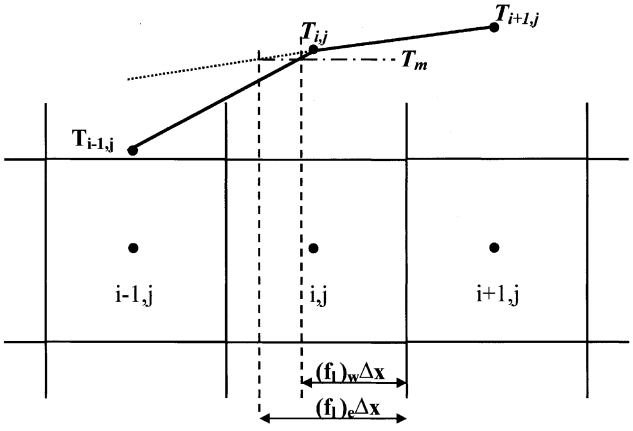

Fig. 2. Calculation of liquid fraction from temperature slopes in liquid and solid.

fraction of any (i, j) cell be allowed to take a negative value when the interface passes the cell boundary and enters $(i+1, j)$ cell. After a converged solution in the iteration process at time step k has been reached, the liquid fraction of the $(i+1, j)$ cell at the next time step $k+1$ is recalculated and the liquid fraction of the (i, j) cell is set to be zero:

$$f_{\mathrm{l}}^{0,k+1}(i+1,j) = 1.0 + f_{\mathrm{l}}^{p,k}(i,j)$$
$$f_{\mathrm{l}}^{0,k+1}(i,j) = 0 \tag{15}$$

2.1.2. Diffusion equation and extrapolation scheme for interface concentration

The source term accounting for the release of solute into the liquid during solidification can be derived by considering an average concentration in a control volume which is undergoing phase change (Voller et al., 1989). This control volume can be treated as partially solidified with an average solute concentration of

$$C = f_{\mathrm{s}} C_{\mathrm{s}} + f_{\mathrm{l}} C_{\mathrm{l}} \tag{16}$$

where $f_{\mathrm{s}} = 1 - f_{\mathrm{l}}$ is the local solid volume fraction. Since diffusion in the solid is neglected, the concentration in the solid remains constant over time at any position, although it may and generally will change with position in the solid as solidification proceeds. The solute conservation equation can be written

$$\frac{\partial C_{\mathrm{l}}}{\partial t} + \nabla \cdot (\widetilde{V} C_{\mathrm{l}}) = \nabla \cdot (D \nabla C_{\mathrm{l}}) + S_C \tag{17}$$

in which

$$S_C = \frac{\partial f_{\mathrm{s}}}{\partial t}(1 - k_{\mathrm{p}}) C_{\mathrm{l}} + f_{\mathrm{s}} \frac{\partial C_{\mathrm{l}}}{\partial t} \tag{18}$$

where k_{p} is the partition coefficient ($C_{\mathrm{s}}/C_{\mathrm{l}}$ at the interface). Note that S_C is zero throughout the liquid except at the interface (i.e., in the partially solidified control volume adjacent to the interface).

During solidification, the melting temperature varies due to changes in solute concentration. With the assumption that phase change takes place under local thermodynamic equilibrium, the temperature at the interface, i.e., the melting temperature T_{m}, can be expressed

$$T_{\mathrm{m}} = T_{\mathrm{m0}} + m_{\mathrm{l}} C_{\mathrm{I}} \tag{19}$$

where T_{m0} is the melting temperature of pure solvent (bismuth, in the case of MEPHISTO-4), m_{l} is slope of the liquidus, assumed to be constant and obtained from the phase diagram and C_{I} is the interface solute concentration in the liquid.

In a fixed-grid formulation, the computed values of C_{l} obtained from Eq. (17) are averaged values over a liquid portion of the partially solidified control volume. As the interface moves from one cell to the next, this average value suddenly decreases because of the finite discretization. It then gradually increases as solidification proceeds due to solute rejection at the interface, which occurs (in the case of Bi–Sn) at a rate faster than diffusion out of the control volume. It follows that the concentration-dependent melting temperature, if calculated from the average concentration, will have an incorrect zigzag shape and hence will not be suitable for the calculation of the local liquid fraction or for the estimation of the interface position. To overcome this problem, it is necessary to calculate the concentration-dependent melting temperature based on the correct interface solute concentration extrapolated from the cell average values.

The concentration gradients near the interface induced by the low values of partition and diffusion coefficients are very sharp. Hence the interface concentration cannot be obtained accurately by linear extrapolation from the average cell concentrations even assuming that the position of the interface has already been accurately predicted. Noting from one-dimensional theoretical considerations that the solute build-up in front of the interface can be described by an exponential function, an extrapolation scheme based on a one-parameter approach (Timchenko et al., 2000) has been suggested. The disadvantage of this scheme is that it requires a knowledge of the rate of solidification and hence the extrapolation procedure needs to be adjusted to account for different rates. A three-point extrapolation scheme was used in Chen et al. (1998). However this extrapolation procedure produces an interface concentration which may not be continuous when the interface passes through a cell boundary. This can produce a discontinuity in the melting temperature and hence in the position of the interface when concentration-dependent melting temperature is taken into account.

We now present an extrapolation scheme given by

$$C_{\mathrm{I}} = C_{i,j}(1 + f_{\mathrm{l}}\alpha) \tag{20}$$

The parameter α is determined, as described below, from the maximum (last) value of $C_{i-1,j}$ which occurs before cell $(i-1, j)$ becomes completely solidified and the minimum (first) value of $C_{i,j}$ calculated when the interface moves into the cell (i, j)

$$\alpha = \left\{(C_{i-1,j})_{\mathrm{last}} - (C_{i,j})_{\mathrm{first}}\right\} / \left\{(f_{\mathrm{l}})_{\mathrm{first}}(C_{i,j})_{\mathrm{first}}\right\} \tag{21}$$

This formulation ensures that when the interface first enters the new cell (i, j), the interface concentration is equal to that when the interface was about to leave the cell $(i-1, j)$ and hence that C_{I} remains a monotonically increasing function when the interface goes from one computational cell to the next during solidification, i.e.

$$C_{\mathrm{I}} = (C_{i,j})_{\mathrm{first}}\left\{1 + (f_{\mathrm{l}})_{\mathrm{first}}\alpha\right\} = (C_{i-1,j})_{\mathrm{last}} \tag{22}$$

When the cell becomes completely solidified ($f_l(i,j)$ approaches zero) from Eq. (20) it can be seen that $C_I = C_{i,j}$.

To account for the interface movement through the partially solidified control volume, the diffusion flux in the direction of solidification was discretized in the manner described in Timchenko et al. (2000).

2.1.3. Translation of adiabatic boundary conditions

In Timchenko et al. (2000) we considered a Bridgman furnace in which a moving temperature profile, consisting of a cold zone (T_c), a transition zone and a hot zone (T_h), was imposed at the liquid boundary. Conduction in the ampoule was not considered and the transition zone simulated the nominally adiabatic region between the cold and hot zones by the imposition of a ramp temperature profile with a specified constant gradient at the liquid boundary. In more recent work (Timchenko et al., 2001) and including the present paper we have included heat conduction in the ampoule, which in MEPHISTO is made of quartz, as part of the calculation procedure, and have imposed a temperature gradient of 27 K/mm on the *outside* of the ampoule. This leads to an internal gradient of approximately 20 K/mm, corresponding to the gradient achieved in the experiments. The next improvement was to incorporate true adiabatic conditions into the model. The experiment sought to achieve an adiabatic region between the cold and hot jackets, although there must inevitably have been some conduction in the structure of the jackets militating against this. Apart from being more realistic, there is a computational reason for using adiabatic conditions: the imposition of a linear temperature profile in a nominally adiabatic zone led to a larger interface curvature and concentration segregation than was expected.

To be able to use an extrapolation scheme for concentration, we need to obtain a smooth decrease in the temperature of the partially solidified cell as the interface moves through the cell. However, translation of an isothermal boundary condition and an adjacent adiabatic boundary condition does not generate a smooth change in the boundary temperature, because the boundary cell at the junction between the two conditions must be treated as either isothermal or adiabatic depending on where the junction lies with respect to the grid point. Because the boundary condition is implemented on discrete points, this change cannot take place continuously in time. In order to achieve a continuous translation of the adiabatic boundary condition along a fixed-grid boundary, therefore, a weighted boundary condition was used for the boundary cell containing this junction point.

Consider a junction with a cold isothermal condition to its left and an adiabatic condition to its right, during an event in which the temperature profile is moving to the right. Until the junction point crosses the boundary of this cell, the cell experiences an adiabatic boundary condition. The cell boundary temperature T_w is calculated from the first two internal liquid temperatures (denoted here by T_1 and T_2) using a second-order approximation to the zero wall heat flux. In the case of a uniform mesh of size Δy this flux is:

$$q_w = \frac{-3T_w + 4T_1 - T_2}{2\Delta y} = 0 \tag{23}$$

When the junction point enters the cell, this cell becomes partially under adiabatic and partially under isothermal boundary conditions. To account for this, the following expression is used to calculate the nodal boundary temperature:

$$T_w = F(T_1, T_2)(1 - \xi) + T_c\xi \tag{24}$$

where $F(T_1, T_2) = (4T_1 - T_2)/3$ and ξ is the distance from the left (solid side) cell boundary to the junction point expressed as a fraction of the mesh size. When ξ is zero, the cell is fully adiabatic; when it is unity, the cell is fully isothermal. The same approach is applied to the movement of the junction point between the adiabatic and hot isothermal zones.

The treatment of temperatures at the boundary between the ampoule and the solidifying alloy required the implementation of a special numerical scheme in SOLCON. An additional equation for T_b was constructed by integrating the differential equation over the half control volume adjacent to the boundary. Perfect thermal contact at the alloy/ampoule interface is assumed, so that the conductive flux across the boundary is constant:

$$q_b = k_m \left.\frac{\partial T}{\partial n}\right|_m = k_{amp} \left.\frac{\partial T}{\partial n}\right|_a \tag{25}$$

where subscript "m" denotes the alloy material in both liquid and solid phases, and "*amp*" denotes the ampoule. The heat flux q_b written in terms of ampoule temperatures is used as the source term in the equation for the boundary temperatures. This allows the inclusion of alloy/ampoule boundary temperatures in the solution procedure for the solidifying sample temperatures. The ampoule outer boundary temperatures are calculated using Eq. (24) and used for the calculation of internal ampoule temperatures in the next iteration.

3. Solution methods

Two different solution methods were used. One is a finite difference vorticity–stream function formulation implemented in an in-house code called SOLCON [4] and another uses a finite volume, primitive variable formulation in the commercial code CFX (CFX 4.2:

[4] Solidification and convection.

Solver, 1997), which is a general purpose code designed so that complex three-dimensional geometries may be readily handled. Although it can be used for two-dimensional problems (by selecting a mesh size of three in the 'third' direction), it tends to be more demanding in CPU time than a purpose-written 2-D code.

3.1. SOLCON

A modified Samarskii–Andreyev (ADI) scheme was used to solve iteratively the vorticity, stream function, energy and solute equations at each time step. The modification was designed to ensure accurate coupling between the solution of the transient equations and the thermal boundary conditions and to achieve true transient "simultaneous" solution of the equations. The coupling between equations and boundary conditions becomes especially important because of the movement of the temperature boundary profile. Moreover, the use of iterations is necessary because of the strong non-linearity of all governing equations. To ensure stability of the computational process, all source terms and non-linear coefficients depending on liquid fraction were linearized based on the value of the liquid fraction obtained from the previous iteration. In the solid, the vorticity, stream function and velocities were set to zero.

The vorticity, stream function and energy equations were discretized using central differences and solved by this modified ADI scheme. Interface boundary conditions for vorticity and stream function were applied at the mesh points in the solid sub-region nearest to the s/l interface. Following Raw and Lee (1991) for the calculation of vorticity boundary conditions, the expression

$$\zeta = (\sin^{-2}\gamma)\partial^2\psi/\partial x^2 \tag{26}$$

was used. Here γ is the angle between the liquid/solid interface and the horizontal axis. The boundary condition $\psi = 0$ was used for the stream function. The concentration Eq. (17) was discretized using a control volume approach to ensure mass balance during phase change in the partially solidified control volume. A second-order upwind scheme was used for the convection fluxes with central differences for the diffusion terms.

3.2. CFX

A sequential solution algorithm using the commercial flow code CFX with a primitive variable formulation was used. In order to simulate the solid region in which the velocity is zero, a resistive force R was introduced into the momentum equation. R was set to zero in the liquid and was given a very large value in the solid (typically 10^6). The set of transport equations was discretized using a finite volume method. The SIMPLEC algorithm was used for pressure–velocity coupling with the Rhie–Chow interpolation method to prevent oscillations of pressure on the non-staggered grid. A fully implicit scheme was used for marching in time. Discretization of convection fluxes was performed using a hybrid scheme and the diffusion fluxes were discretized using central differences. The full field Stone's method was used to solve the complete system of equations.

4. Results and discussion

4.1. Comparisons with analytical solutions

To validate the physical and mathematical models, a comparison of numerical results (C_n) with the analytical solution (C_a) of Smith et al. (1955) for one-dimensional, diffusion-controlled plane front solidification was performed. No convection was included. Results of this comparison are shown in Fig. 3. It can be seen that the computed solute concentrations in the solid at the mid-height of the ampoule are very close to the analytical, diffusion-controlled values. The relative difference $(C_a - C_n)/C_a$ is less than 1%. As noted below, segregation occurs and the concentrations away from the mid-height would differ from these one-dimensional values. Fig. 4 shows liquid cell average concentration (solid line) and extrapolated interface concentration (dashed line), which was used to calculate the solid concentration shown in Fig. 3.

4.2. Modelling of MEPHISTO experiments

For the solutions presented here, grid sizes of 0.2 and 0.5 mm in the x (axial) and y (transverse) directions respectively, and times steps of 1 s were typically used in

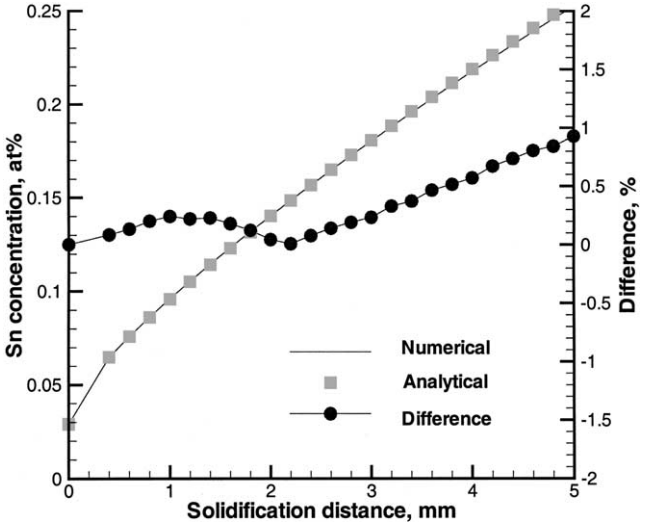

Fig. 3. Analytical and numerical solute concentration in the solid for 5 mm of solidification.

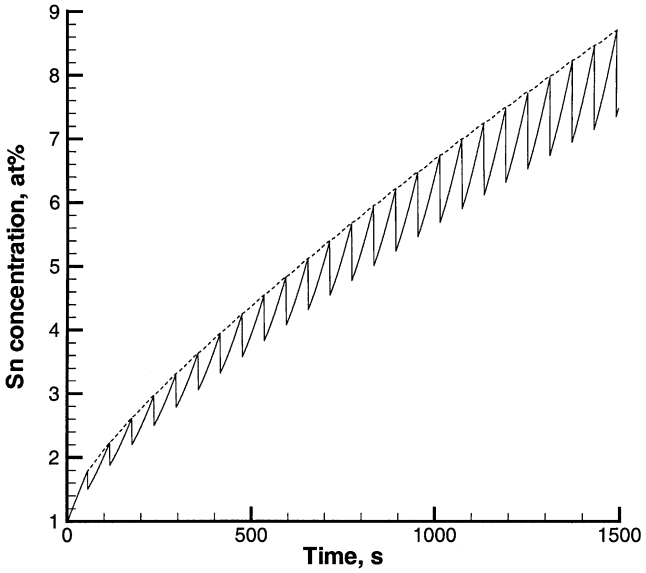

Fig. 4. Time history of computed liquid cell average concentration (—) and extrapolated interface concentration (- - -).

CFX. For SOLCON a grid size of 0.2 mm in the x and 0.3 mm in y directions was used with time step of 0.5 s. These mesh sizes were found to be adequate by extensive testing against results obtained using finer meshes.

The model has been applied to the simulation of the experiments performed during the 1997 flight of MEPHISTO-4. In the example described below (the events identified in the flight schedule as 11E and 11F, Abbaschian et al., 2001) solidification at a pulling speed (the speed of the moving furnace) of 3.34 μm/s occurred for 0.333 h. The furnace was then stopped for 3.7 h (an "extended hold") during which time almost complete rehomogenization of the liquid occurred. Solidification at a speed of 1.85 μm/s followed for 0.6 h. The melting temperature was calculated according to (21) with $m = -2.32$ K/at.%. The magnitude of the gravity vector was taken to be 1 μg, i.e., 9.81×10^{-6} m s^{-2}, acting in a direction normal to the axis of the ampoule. The variation of the thermal conductivity between the solid and liquid phases was taken into account with

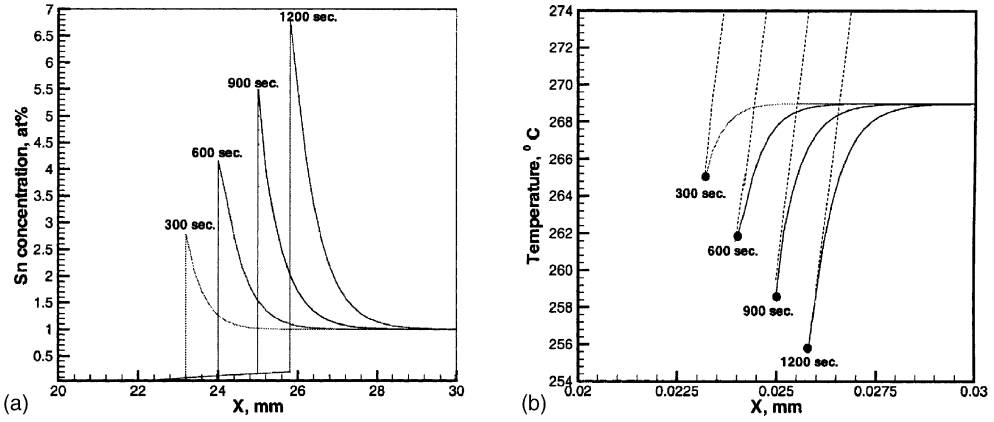

Fig. 5. (a) Distribution of solute concentration at the mid-height of the ampoule during event 11E. (b) Distribution of melting temperature (—) and the actual temperature distribution (- - -) at the mid-height of the ampoule during event 11E.

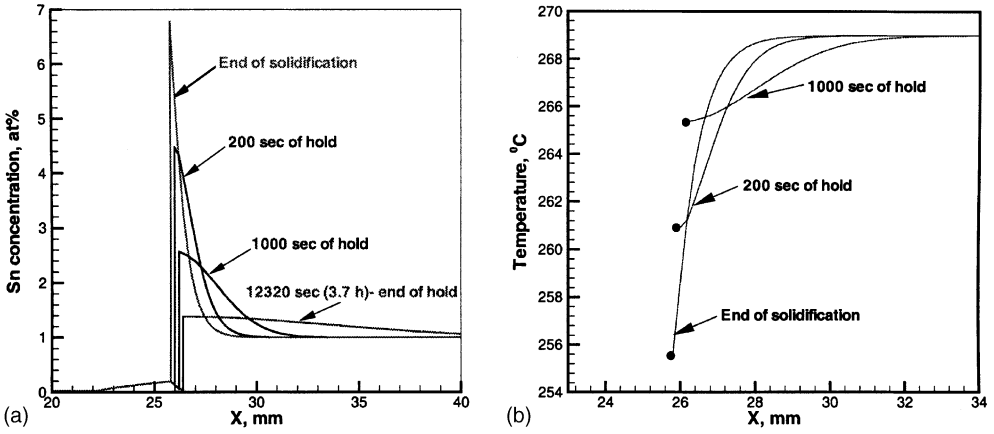

Fig. 6. (a) Distribution of solute concentration at the mid-height of the ampoule during the hold. (b) Distribution of melting temperature at the mid-height of the ampoule during the hold.

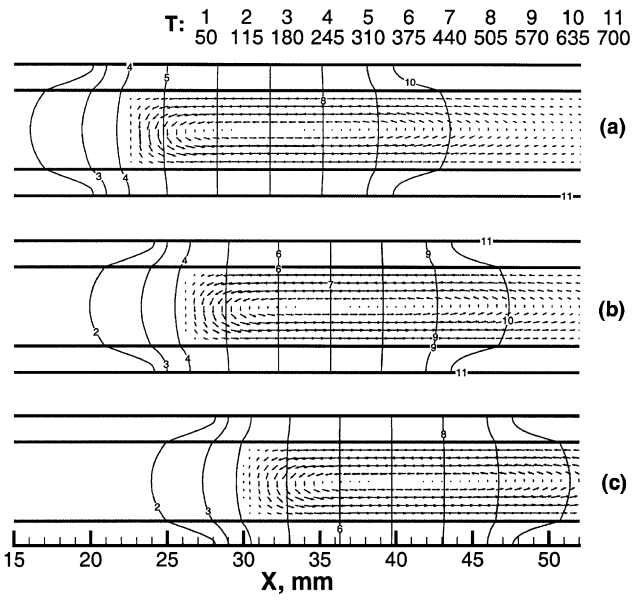

Fig. 7. Temperature contours and velocity field (a) at the start of solidification, (b) at the end of event 11E and (c) after event 11F.

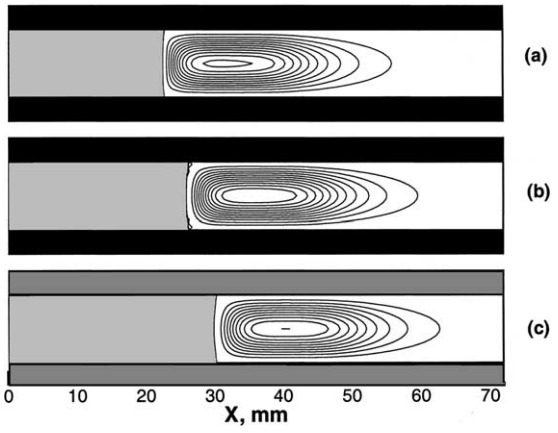

Fig. 8. Stream function contours and s/l interface (a) at the start of solidification, (b) at the end of event 11E and (c) after event 11F.

$k_l = 12.4$ W/m K and $k_s = 6.5$ W/m K. Properties values for pure liquid bismuth (Timchenko et al., 1998) taken at the reference temperature of 271.3 °C (the equilibrium melting temperature of Bi) were used. The partition coefficient k_p for Sn in Bi was taken to be 0.029. Reported values of the diffusion coefficient D for dilute Sn in Bi near 271.3 °C vary from 1.76×10^{-9} m^2/s (Buell and Shuck, 1970) to 2.7×10^{-9} m^2/s (Niwa et al., 1957). In these calculations $D = 2.0 \times 10^{-9}$ m^2/s was chosen after a comparison of numerical solutions with post-flight microprobe results for solute concentration in the solid.

The moving temperature profile imposed on the outer walls of the ampoule consisted of a cold zone ($T_c =$ 50 °C), an adiabatic zone and a hot zone ($T_h = 700$ °C). The length of the adiabatic zone was 20 mm, leading to an internal temperature gradient in the liquid of approximately 20 K/mm.

Fig. 5(a) shows the distribution of solute concentration at the mid-height of the ampoule during the 11E solidification event. Fig. 5(b) shows the distribution of melting temperature (solid lines) and the actual temperature distribution (dashed lines) at the mid-height of the ampoule during the same event. Because of the increase of solute concentration at the interface during solidification, the melting temperature decreases according to the slope of liquidus in the phase diagram (Eq. (19)). During the hold, solute concentration at the interface decreases due to diffusion of solute into the liquid as shown in Fig. 6(a). Accordingly, the melting temperature increases as shown in Fig. 6(b).

Fig. 7 shows temperature contours and the velocity field in the liquid phase (a) at the start of solidification, (b) in the end of event 11E and (c) after event 11F. It can be seen that both temperature and velocity fields are moving along the sample as time progresses according to the moving boundary temperature profile.

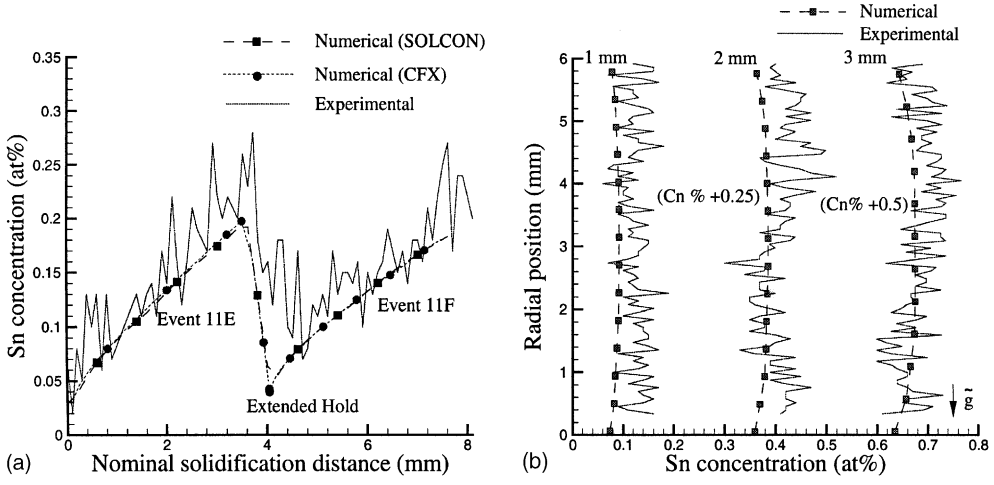

Fig. 9. Solute concentration in the solid (a) along the ampoule centre line and (b) across the ampoule.

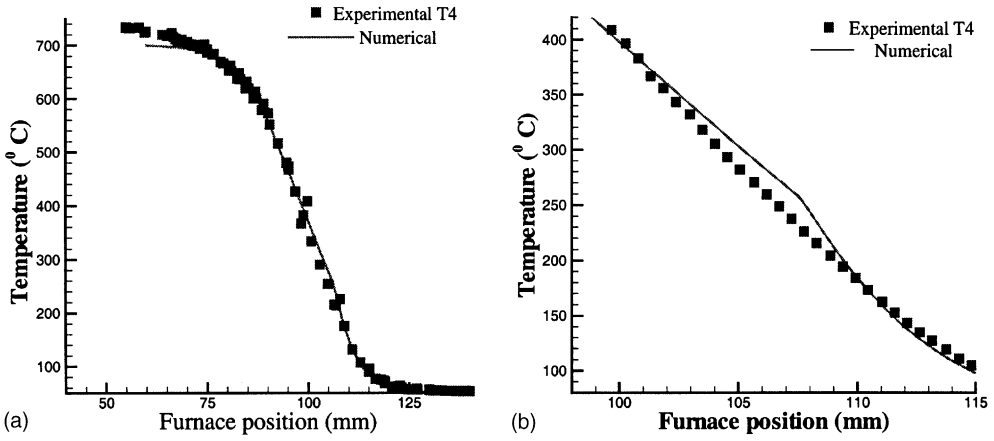

Fig. 10. Temperature distribution (a) along the centre line and (b) in the vicinity of interface.

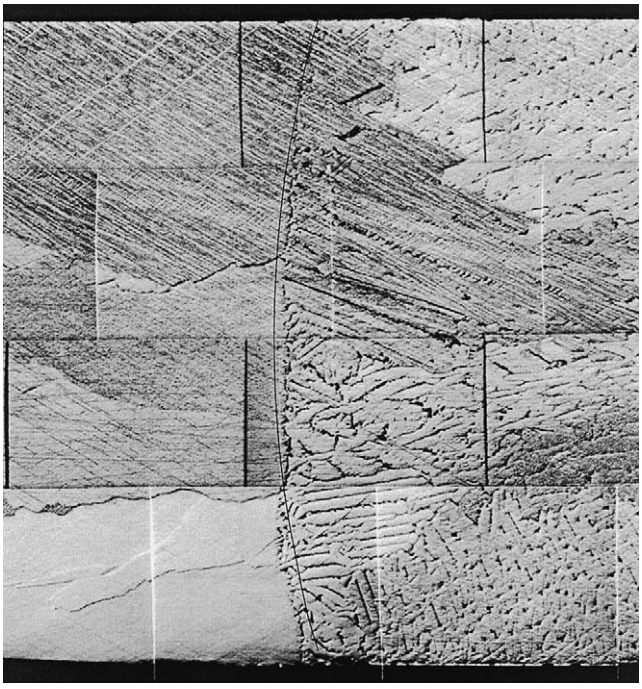

Fig. 11. Comparison of the computed and measured interface shape.

Fig. 8 shows the s/l interface and stream function contours in the liquid at the same times as shown on Fig. 7. The flow is thermally driven and counterclockwise. At the end of the 11E solidification, a very weak positive vertical velocity has appeared near the interface in the top and bottom corners due to convection induced by solutal gradients. During the hold, gradients of the concentration in front of the interface dropped substantially (Fig. 6(a)) and a reverse cell has not formed.

The distribution of solute concentration in the solid along the centre line of the sample is shown in Fig. 9(a). Numerical solutions are presented together with the microprobe results obtained after the flight from the experimental samples. Fig. 9(b) shows the distribution of solute concentration across the solid. Both axial and transverse numerical distributions are in very good agreement with the experimental results.

Due to limitations in the measurement of temperature, some discrepancy did exist between computed and measured temperatures. Fig. 10(a) shows the computed temperature distribution along the centreline of the sample together with the in-flight measurements obtained using a thermocouple located on the centre line. Fig. 10(a) contains measurement data obtained from all events; finer details of the temperature distribution near the interface taken from one event are shown in Fig. 10(b). The change in the computed temperature gradient is caused by the change in thermal conductivity between the solid and liquid phases. The measurements do not exhibit this sharp change in gradient; a smearing of the experimental values results from the finite size of the thermocouple.

Fig. 11 shows the interface shape after the last event of solidification (11F) in the MEPHISTO experiment. The computed interface shape is in excellent agreement with that observed in the actual experiment.

5. Conclusion

A modified fixed-grid approach has been used to simulate MEPHISTO experiments on the solidification of a bismuth–tin alloy. To obtain a smooth history of the temperature and interface position while the interface is moving through a fixed-grid domain, procedures for the calculation of liquid fraction, interface concentration and translation of adiabatic boundary condition were developed. Comparisons of computed solutions for solute concentration, temperature and interface shape with measured values show very good agreement.

Acknowledgements

The UNSW authors acknowledge with thanks the support of the Australian Research Council and the Australian Department of Industry, Science and Technology. They also express their gratitude to H.C. de Groh III, NASA Glenn Research Center, for the opportunity to participate in MEPHISTO-4 and his continual collaboration during this research.

References

Abbaschian, R., de Groh III, H.C., Leonardi, E., de Vahl Davis, G., Coriell, S., Cambon, G., 2001. Final Report for the Shuttle Flight Experiment on USMP-4: In situ Monitoring of Crystal Growth Using MEPHISTO. NASA Technical Publication., NASA/TP-2001-210825.

Buell, C., Shuck, F., 1970. Diffusion in the liquid Bi–Sn system. Metall. Trans. 1, 1875–1880.

Chen, P.Y.P., Timchenko, V., Leonardi, E., de Vahl Davis, G., de Groh III, H.C., 1998. A numerical study of directional solidification and melting in microgravity, HTD-vol. 361-3/PID-vol. 3. Proc. of the ASME Heat Transfer Division—vol. 3, Nelson Jr., R.A., Swanson, L.W., Bianchi, M.V.A., Camci, C., (Eds.), ASME, New York, pp. 75–83.

CFX 4.2: Solver, 1997. CFX International, Didcot, OX11 ORA, UK.

Laouadi, A., Lacroix, M., Galanis, N., 1998. A numerical method for the treatment of discontinuous thermal conductivity in phase change problems. Int. J. Numer. Meth. Heat Fluid Flow 8, 265–287.

Niwa, K., Shimoji, M., Kado, S., Watanabe, Y., Yokokawa, T., 1957. Studies of diffusion in molten metals. AIME Trans. 209, 96–101.

Raw, W.Y., Lee, S.L., 1991. Application of weighting function scheme on convection–conduction phase-change problems. Int. J. Heat Mass Transfer 34, 1503–1513.

Rouzaud, A., Favier, J.J., Thevenard, D., 1988. A space instrument for fundamental materials science problems: the MEPHISTO program. Adv. Space Res. 8 (12), 49–59.

Smith, V.G., Tiller, W.A., Rutter, J.W., 1955. A mathematical analysis of solute redistribution during solidification. Can. J. Phys. 33, 723–743.

Tacke, K., 1985. Discretization of the explicit enthalpy method for planar phase change. Int. J. Numer. Meth. Eng. 21, 543–554.

Timchenko, V., Chen, P.Y.P., de Vahl Davis, G., Leonardi, E., 1998. Directional solidification in microgravity. In: Lee, J.S. (Ed.), Heat Transfer 98. Taylor & Francis, London, pp. 241–246.

Timchenko, V., Chen, P.Y.P., de Vahl Davis, G., Leonardi, E., Abbaschian, R., 2000. A computational study of transient plane front solidification of alloys in a Bridgman apparatus under microgravity conditions. Int. J. Heat Mass Transfer 43, 963–980.

Timchenko, V., Chen, P.Y.P., de Vahl Davis, G., Leonardi, E., Abbaschian, R., 2001. A numerical study of the MEPHISTO experiment. In: de Vahl Davis, G., Leonardi, E. (Eds.), CHT'01 Advances in Computational Heat Transfer II. Begell House Inc., New York, pp. 1089–1096.

Voller, V.R., Brent, A.D., Prakash, C., 1989. The modelling of heat, mass and solute transport in solidification systems. Int. J. Heat Mass Transfer 32, 1719–1731.

Voller, V.R., Fabbri, M., 1995. Numerical solution of plane-front solidification with kinetic undercooling. Numer. Heat Transfer, Part B 32, 467–486.